INTERNATIONAL JOURNAL FOR NUMERICAL METHODS IN FLUIDS
Int. J. Numer. Meth. Fluids **30**: 635–652 (1999)

REVERSE ROLL COATING FLOW

YUE HAO AND SHIMON HABER*

Faculty of Mechanical Engineering, Technion-Israel Institute of Technology, Technion City, Haifa 32000, Israel

SUMMARY

The Galerkin finite element method of solution formulated by Coyle *et al.* is applied to analyse the coating flow field between two reverse rotating rolls. A wide range of operating conditions that are of practical importance were studied. Many quantitative results that can benefit a practising engineer are presented and physical insight is gained by the analysis of the data. It is shown that the reverse roll coating process is affected by various factors, among which the roll speed ratio is the most significant. Regardless of other parameters chosen, a critical speed ratio always exists at which the metered film thickness experiences a minimum. At this critical speed ratio, the dynamic contact line is exactly located at the centre of the gap between the two rolls. The significance of the Reynolds and the Capillary numbers increases with increasing speed ratio. For speed ratios beyond the critical value, a thinner metered film can be achieved by means of either increasing the film thickness of the entering layer or by decreasing the principal roll radius. Furthermore, the computational predictions indicate that changing the roll radius ratio has no obvious effect on reverse roll coating and that gravity effects, quantified by the Stokes number, can be ignored under normal operating conditions. Copyright © 1999 John Wiley & Sons, Ltd.

KEY WORDS: coating flow; reverse roll; free surface; thin film

1. INTRODUCTION

Roll coating is an important and common coating process widely used in the areas of tape, film and printing industry. Roll coating process, in which the nip distance between the two rotating rolls is much smaller than the rolls radii, is usually classified into forward roll coating, reverse roll coating and metering roll coating [1,2] as shown in Figure 1. In forward roll coating, the two rolls move in the same direction at the nip. The coating liquid forms a pool on the upstream side of the nip and separates into two liquid films covered on the two roll surfaces after leaving the nip, one of which is applied to the substrate for the industrial purpose (Figure 1(a)). In both reverse roll coating and metering coating, the rolls move in opposite directions at the nip. For reverse roll coating (Figure 1(b)), the leakage liquid flux through the nip is recycled and the transferred flow flux is applied on the substrate, while for metering roll coating (Figure 1(c)), the leakage flow flux forms the uniform metered film on the substrate. It can be seen that for these two coating processes, the configurations of the flow field between two rotating rolls are identical. Therefore, both of them are generally called reverse roll coating system. Higgins [3], Booth [4] and Coyle *et al.* [5,6] also presented the general description of this industrial coating technique and its applications.

* Correspondence to: Faculty of Mechanical Engineering, Technion-Israel Institute of Technology, Technion City, Haifa 32000, Israel.

CCC 0271–2091/99/140635–18$17.50

Received 2 September 1997
Accepted 19 May 1998

Over the past 60 years, the flow problems of roll coating processes have been under extensive investigation, which included experimental, analytical and computational analyses. Among them, forward roll coating was central and the most frequently addressed topic. Experimental investigations on it were carried out by Benkreira *et al.* [1,2], Greener and Middleman [7] and Decré *et al.* [8], whereas theoretical analyses were presented by Benkreira *et al.* [1,11], Greener and Middleman [7], Pitts and Greiller [9], Hintermaier and White [10],

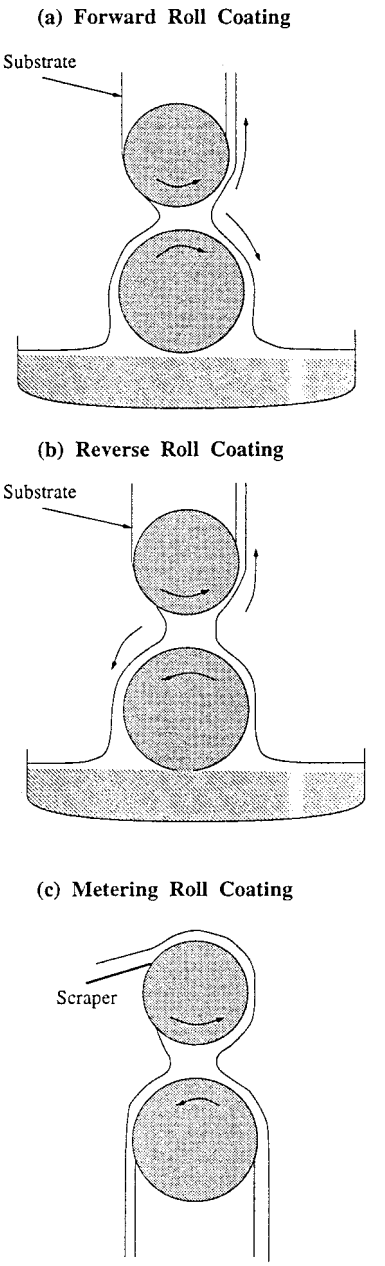

Figure 1. Schematic of roll coating processes.

Coyle *et al*. [12,13], Gaskell *et al*. [14] and Carvalho and Scriven [15]. Compared with forward roll coating, reverse roll coating studies have attracted much less attention. In the earlier works by Ho and Holland [16] and Greener and Middleman [17], lubrication theory was applied to investigate reverse roll coating systems, ignoring the effects of surface tension, the presence of free surfaces and dynamic contact lines. Coyle *et al*. [5,6] have examined this model by both experimental and numerical methods and manifested that the lubrication model fails at high roll speed ratios. The most recent progress on reverse roll coating can be attributed to numerical simulations. Coyle *et al*. [5] applied a finite element method that was supported by experimental results to demonstrate the basic fluid dynamic features of reverse roll coating. They also explained the occurrence of flow instabilities, such as ribbing and cascading. To date, their work is the most advanced investigation on reverse roll coating that closely predicts experimental observations. Nevertheless, since Coyle *et al*. [5] focused on the instability behaviours of reverse roll coating, their experimental and computational results do not cover the whole range of operating conditions or parameters that might be of significance in industrial applications.

The main objective of this paper is to provide a more detailed and comprehensive description of reverse roll coating flows accounting for all the parameters affecting the coating process, and in particular those of great practical significance. To achieve this goal we apply the numerical scheme devised by Coyle *et al*. [5]. Extension of that scheme to a wider variety of flow parameters is by no means trivial. It entails solving a highly non-linear problem in which an initial good 'guess' for the location of the free surfaces is a requisite to obtaining convergent results. The most difficult and laborious task is to create a database that includes converging results for several distinct sets of parameters. The numerical scheme is then implemented by changing a single parameter by small increments and using the database values as a first-order iteration.

Although the present work is restricted to stable operating conditions, it may provide valuable information for further studies on instabilities of reverse roll coating flows.

2. THE REVERSE ROLL COATING SYSTEM

The isothermal, steady and two-dimensional coating flow of Newtonian liquids is studied. The system consists of two parallel coating rolls that rotate reversely with a fixed speed ratio (Figure 2). Between the rolls a very narrow gap is maintained. The coating flow is driven into the nip region between the two rolls by reverse roll 1, say, the applicator [5], then it is partly transferred onto the coated film on the forward rotating roll 2, also known as the metering roll and partly passes through the nip region to form the metered film on the applicator surface. The coating flow field is bounded by inlet and outflow boundaries, moving solid surfaces, and upstream and downstream free surfaces along with the dynamic contact line. The free surface shape and the contact line location are *a priori* unknown.

3. GOVERNING EQUATIONS AND BOUNDARY CONDITIONS

For steady, isothermal flow of incompressible liquid, the dimensionless Navier–Stokes equations in divergence form with the corresponding boundary conditions are [12]:

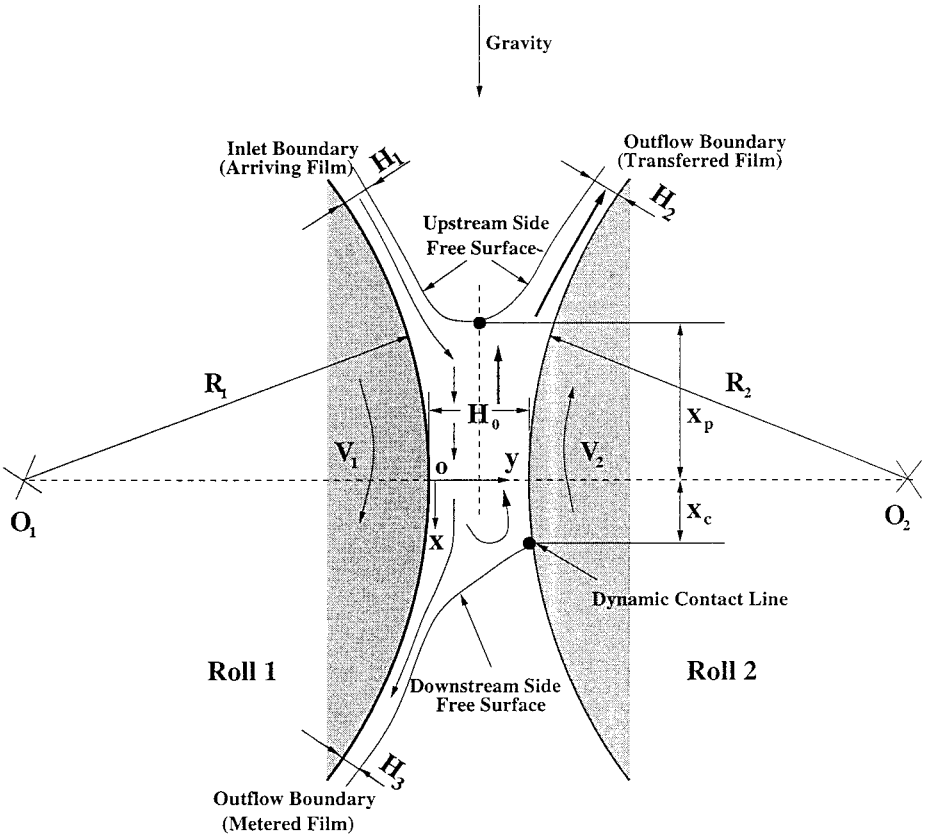

Figure 2. Geometric sketch of the reverse roll coating system.

Continuity equation:

$$\nabla \cdot \mathbf{u} = 0, \tag{1}$$

Momentum equation:

$$Re\nabla \cdot (\mathbf{uu}) = \nabla \cdot \boldsymbol{\tau} + St\mathbf{f}, \tag{2}$$

where for isotropic Newtonian liquids,

$$\boldsymbol{\tau} = -p\mathbf{I} + [\nabla \mathbf{u} + (\nabla \mathbf{u})^T].$$

Here $\mathbf{u}$ and p denote the non-dimensional velocity and pressure fields respectively, and $\mathbf{I}$ is the unit dyadic; $\mathbf{f}$ denotes a unit vector colinear with gravity. Re is the Reynolds number,

$$Re = \frac{\rho V_1 H_0}{\mu}$$

and St is the Stokes number

$$St = \frac{\rho g H_0^2}{\mu V_1}.$$

The Cartesian co-ordinates X, Y, the velocity field $\mathbf{U}$, the pressure P and the total stress $\mathbf{T}$ were non-dimensionalized as follows:

$$x = \frac{X}{H_0}, \quad y = \frac{Y}{H_0}, \quad \mathbf{u} = \frac{U}{V_1}, \quad p = \frac{PH_0}{\mu V_1}, \quad \boldsymbol{\tau} = \frac{\mathbf{T}H_0}{\mu V_1}, \tag{3}$$

where ρ and μ are the fluid density and viscosity respectively, H_0 denotes the minimum gap between two rolls, g is gravity acceleration and V_1 is the circumference velocity of roll 1.

The flow field governed by Equations (1) and (2) satisfies the following boundary conditions.

At the roll surfaces and the inlet boundary,

$$\mathbf{u} = \mathbf{u}_s \tag{4}$$

and

$$\mathbf{u} = \mathbf{u}_{in} \tag{5}$$

respectively, where subscripts s and in represent the solid surface and the inlet boundary respectively.

No-traction condition

$$\mathbf{n} \cdot \boldsymbol{\tau} = 0 \tag{6}$$

is assumed at the outflow boundary.

At the free surface, the normal stress is required to balance the capillary pressure

$$\mathbf{n} \cdot \boldsymbol{\tau} = \frac{1}{Ca} \frac{\mathrm{d}\mathbf{t}}{\mathrm{d}s} - \mathbf{n}P_a. \tag{7}$$

For the sake of simplicity, ambient pressure P_a is taken to be absorbed in pressure p, and Equation (7) is rewritten as

$$\mathbf{n} \cdot \boldsymbol{\tau} = \frac{1}{Ca} \frac{\mathrm{d}\mathbf{t}}{\mathrm{d}s}, \tag{8}$$

where $\mathbf{n}$ and $\mathbf{t}$ are the unit vectors normal and tangential to the bounary surface respectively, and $\mathrm{d}\mathbf{t}/\mathrm{d}s$ accounts for the curvature of the free surface, with s the arc length along the free surface. The capillary number is the ratio between viscous and surface tension forces:

$$Ca = \frac{\mu V_1}{\sigma},$$

where σ is the surface tension.

The kinematic boundary condition

$$\mathbf{n} \cdot \mathbf{u} = 0 \tag{9}$$

requires no mass flow through the free surface, which constitutes another governing equation for the free surface locations.

The presence of a dynamic contact line somewhat complicates the flow problem. A no-slip hypothesis will cause non-integrable stress singularity to exist over the solid surface near to the contact line [18–22]. In order to circumvent this difficulty, the often used assumption at the contact line is

$$\mathbf{u} = 0. \tag{10}$$

Coyle *et al.* [5] and Kistler and Scriven [23,24] suggested applying the Navier boundary conditions, namely that the flux of momentum tangential to the solid surface be proportional to the velocity discontinuity or local slip velocity,

$$B^{-1}\mathbf{t}_s\cdot(\mathbf{u}-\mathbf{u}_s)=\mathbf{t}_s\mathbf{n}_s:\tau, \tag{11}$$

where B is the dimensionless slip length

$$B=\frac{\beta\mu}{H_0},$$

$\mathbf{t}_s$ and $\mathbf{n}_s$ are unit vectors parallel and perpendicular to the solid surface and $\mathbf{u}_s$ is the solid velocity at the contact line. The product of the local slip coefficient β and liquid viscosity μ characterizes the slip length. Adding the essential condition for the normal velocity component

$$\mathbf{n}_s\cdot\mathbf{u}=0 \tag{12}$$

completes the set of boundary conditions that the velocity field satisfies in the slip region.

To account for the free surface curvature near the contact line, the apparent contact angle θ_c between the unit vector normal to the solid surface $\mathbf{n}_s$ and that to the free surface $\mathbf{n}_f$ must be specified [23,24,5]

$$\mathbf{n}_s\cdot\mathbf{n}_f=\cos\theta_c. \tag{13}$$

The slip length and the apparent contact angle can normally be obtained by experiment. In this analysis, both of them are conjectured since there is no available experimental data at hand. The final solution sensitivity to changes in the latter parameters is analysed in the next section.

4. FINITE ELEMENT ANALYSIS

Due to its topological flexibility, particularly well-suited to coping with irregular domains and the highly deformed free surface boundary, the Galerkin finite element method is applied here. In this work, the spine approach, which was first brought into use by Ruschak [25] and later employed in free surface coating flow by Kistler and Scriven [23,24], is adopted to parameterize the free surfaces and tessellate the physical domain into finite elements. Isoparametric mappings transform the deformed physical domain into a regular computational domain (see Figure 3). The Galerkin weighted residuals of the continuity and momentum equations (1) and (2) and the kniematic condition (9) at the free surface, along with the corresponding boundary conditions, result in a set of algebraic equations with velocity, pressure and free surface locations as unknowns (see [23,24,26]). The latter are solved simultaneously utilizing Newton's iteration process.

$$\mathbf{J}\Delta\alpha_{n+1}=\mathbf{R}(\alpha_n),\quad \alpha_{n+1}=\alpha_n-\Delta\alpha_{n+1}, \tag{14}$$

where $\mathbf{J}$ is the Jacobian matrix,

$$\mathbf{J}\equiv\frac{\partial\mathbf{R}}{\partial\alpha},$$

α is the vector of finite element coefficients,

$$\alpha\equiv[u^1,\ldots,u^K,\ v^1,\ldots,v^K,\ p^1,\ldots,p^L,\ h^1,\ldots,h^F],$$

$\mathbf{R}$ is the vector of weighted residuals,

$$\mathbf{R}\equiv[R^1_{M,x},\ldots,R^K_{M,x},\ R^1_{M,y},\ldots,R^K_{M,y},\ R^1_C,\ldots,R^L_C,\ R^1_K,\ldots,R^F_K],$$

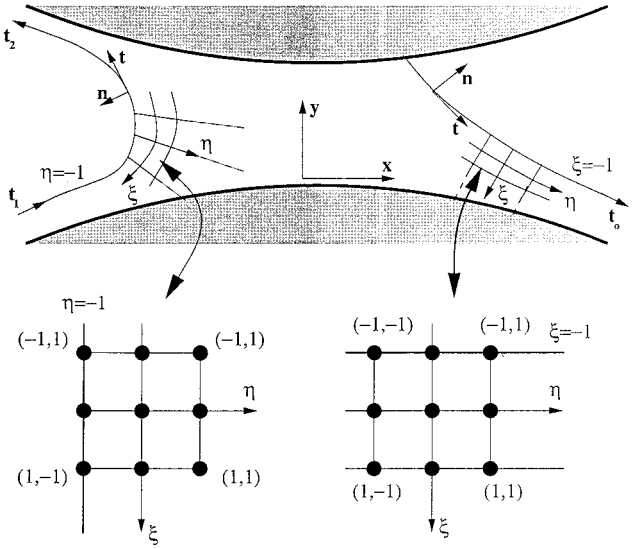

Figure 3. Subisoparametric transformation.

with superscripts L, K and F representing the total numbers of nodes for pressure, velocity and free surface position, and n representing the nth iteration. The iteration proceeds until $\|\Delta\alpha\| < \epsilon$, with ϵ used as a convergent constant.

From each Jacobian matrix at element level (the detailed mathematical formulation of each entry is found in [24])

$$\mathbf{J}^e = \begin{pmatrix} \partial \mathbf{R}^e_{M,x}/\partial \mathbf{u}^e & \partial \mathbf{R}^e_{M,x}/\partial \mathbf{v}^e & \partial \mathbf{R}^e_{M,x}/\partial p^e & \partial \mathbf{R}^e_{M,x}/\partial \mathbf{h}^e \\ \partial \mathbf{R}^e_{M,y}/\partial \mathbf{u}^e & \partial \mathbf{R}^e_{M,y}/\partial \mathbf{v}^e & \partial \mathbf{R}^e_{M,y}/\partial p^e & \partial \mathbf{R}^e_{M,y}/\partial \mathbf{h}^e \\ \partial \mathbf{R}^e_{C}/\partial \mathbf{u}^e & \partial \mathbf{R}^e_{C}/\partial \mathbf{v}^e & 0 & \partial \mathbf{R}^e_{C}/\partial \mathbf{h}^e \\ \partial \mathbf{R}^e_{K}/\partial \mathbf{u}^e & \partial \mathbf{R}^e_{K}/\partial \mathbf{v}^e & 0 & \partial \mathbf{R}^e_{K}/\partial \mathbf{h}^e \end{pmatrix}, \tag{15}$$

the assembly Jacobian matrix $\mathbf{J}$ can be achieved, where $\mathbf{h}$ is the vector of free surface parameters.

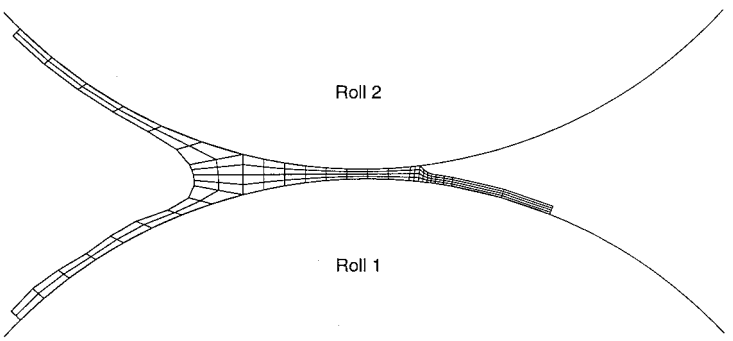

Figure 4. Finite element discretizations.

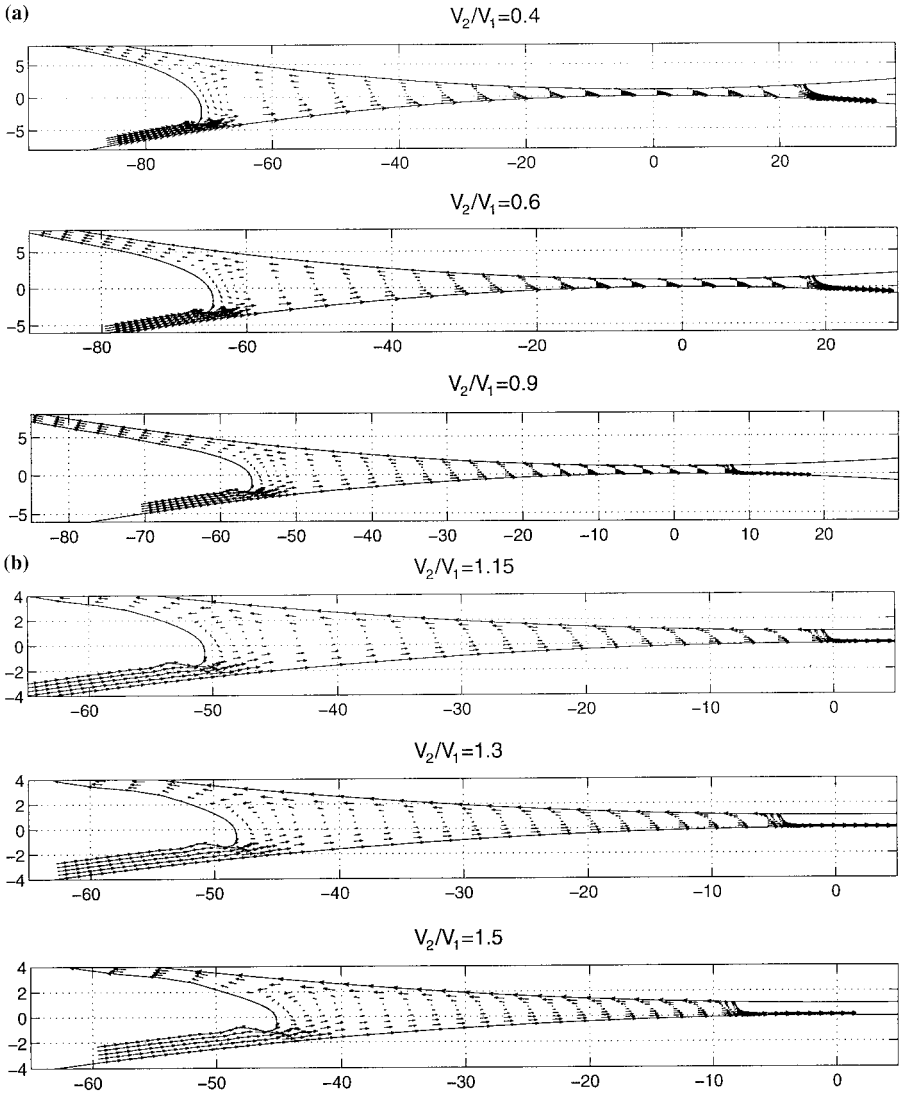

Figure 5. Visualized flow field ($Re = 25$, $Ca = 0.1$, $H_1/H_0 = 1.25$, $R/H_0 = 500$, $R_2/R_1 = 1$ and $St = 0$).

5. THE FINITE ELEMENT SOLUTION AND RESULTS

In this work, the basic selection of the element number in the coating flow region is 104 with the detailed element discretizations shown in Figure 4. Repeated calculations showed that doubling the number of elements had an effect of less than 0.3% on the contact line location. The assembled global stiffness matrix is solved by real linear equation solvers (IMSL: MATH/LIBRARY [27]).

Solutions were obtained to provide a comparatively complete description of reverse roll coating flow with various non-dimensional parameters, such as roll speed ratio (V_2/V_1), Reynolds number (Re), capillary number (Ca), arriving film thickness (H_1/H_0), principal roll radius (R/H_0), roll radius ratio (R_2/R_1) and Stokes number (St). An empirical value of the apparent contact angle θ_c was selected to be 110°.

In reverse roll coating processes, the roll speed ratio plays the most important role. This is vividly illustrated by Figures 5–12. Figure 5 displays how the flow field changes with roll speed ratio. It is found that for low speed ratios, the upstream side free surface and the dynamic contact line are located at either side of the gap centre. Increasing the speed ratio makes the upstream side free surface and the contact line move toward each other. Beyond a certain critical speed ratio, the contact line is pulled through the nip into the upstream side of the gap centre. These findings are also confirmed in Figures 6–12. The metered film thickness H_3/H_0 strongly depends upon the speed ratio V_2/V_1. For low values of the speed ratio, H_3/H_0 is about 0.7. Increasing the speed ratio causes the metered film thickness to drop and reach a minimum value of about 0.16. A further increase of the speed ratio causes the film thickness to rise again. This trend of the metered film thickness was also qualitatively verified by experiment [5].

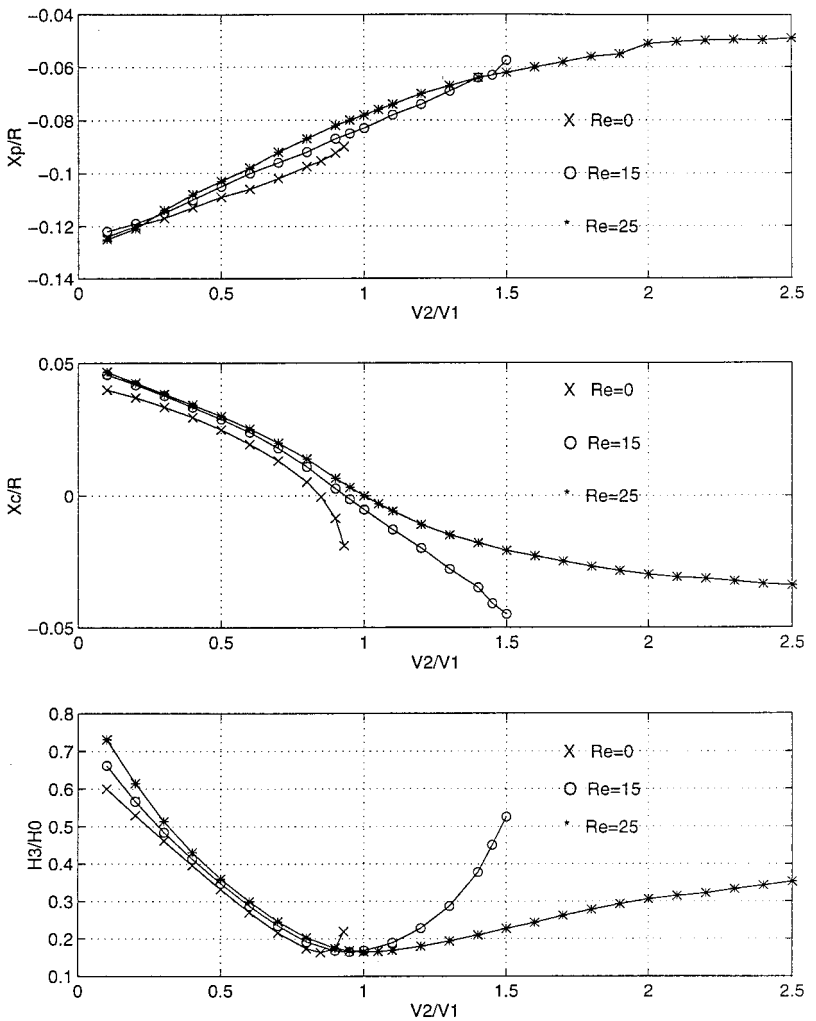

Figure 6. Predicted upstream side free surface position X_p/R, contact line position X_c/R and metered film thickness H_3/H_0 with variations of Reynolds number ($Ca = 0.1$, $H_1/H_0 = 1.25$, $R/H_0 = 1000$, $R_2/R_1 = 1$ and $St = 0$).

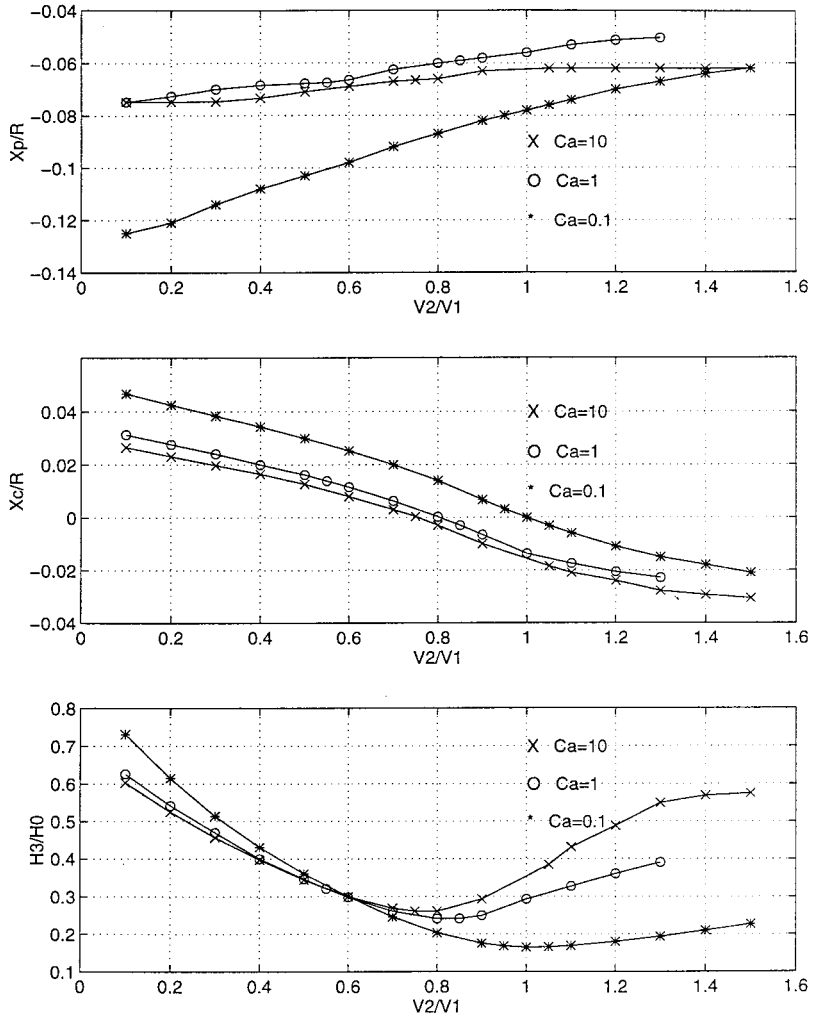

Figure 7. Effects of capillary number on reverse roll coating ($Re = 25$, $H_1/H_0 = 1.25$, $R/H_0 = 1000$, $R_2/R_1 = 1$ and $St = 0$).

For the sake of convenience, the speed ratio at which the film thickness possesses a minimum is henceforth referred to as critical. It is also referred to as the transition point from low to high speed ratios. When the speed ratio reaches that critical value, the contact line lies exactly at the minimum gap between two rotating rolls.

Effects of the Reynolds number on reverse roll coating are clearly shown in Figure 6. The critical speed ratio is lower for smaller values of the Reynolds number and reaches a value of about 0.8 for $Re = 0$. As for low speed ratios, the Reynolds number has little effect; however, for high speed ratios, the metered film thickness and the contact line location are more sensitive to Reynolds number variations. For example, the contact line passes faster through the minimum gap for smaller Reynolds number and the metered film thickness increases sharply as the Reynolds number is reduced.

The capillary number is also an important parameter that greatly influences the coating process. As shown in Figure 7, the larger the capillary number, the lower the critical speed ratio is, while the metered film becomes either thicker at higher speed ratios or thinner at lower speed ratios. For a given speed ratio, increasing the capillary number causes the contact line to locate closer to the upstream side.

Figure 8 reveals the effects of the arriving film thickness on reverse roll coating. The critical speed ratio is not affected, while the upstream side of the transferred layer ensues closer to the minimum gap in case the arriving film thickness decreases. It has no significant effect on either the location of the contact line or the metered film thickness unless the speed ratio exceeds the critical value. In that case, the smaller the arriving film thickness is, the closer the contact line becomes to the upstream side, and the thicker the metered film thickness becomes.

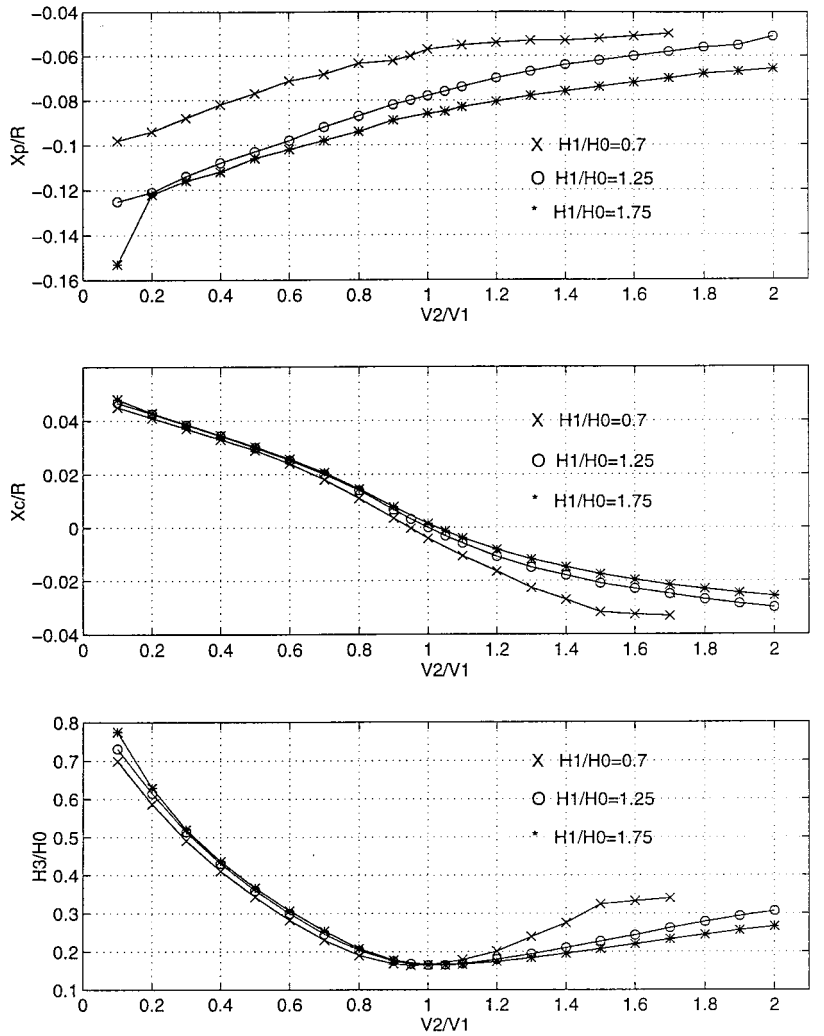

Figure 8. Effects of arriving film thickness H_1/H_0 on reverse roll coating ($Re = 25$, $Ca = 0.1$, $R/H_0 = 1000$, $R_2/R_1 = 1$ and $St = 0$).

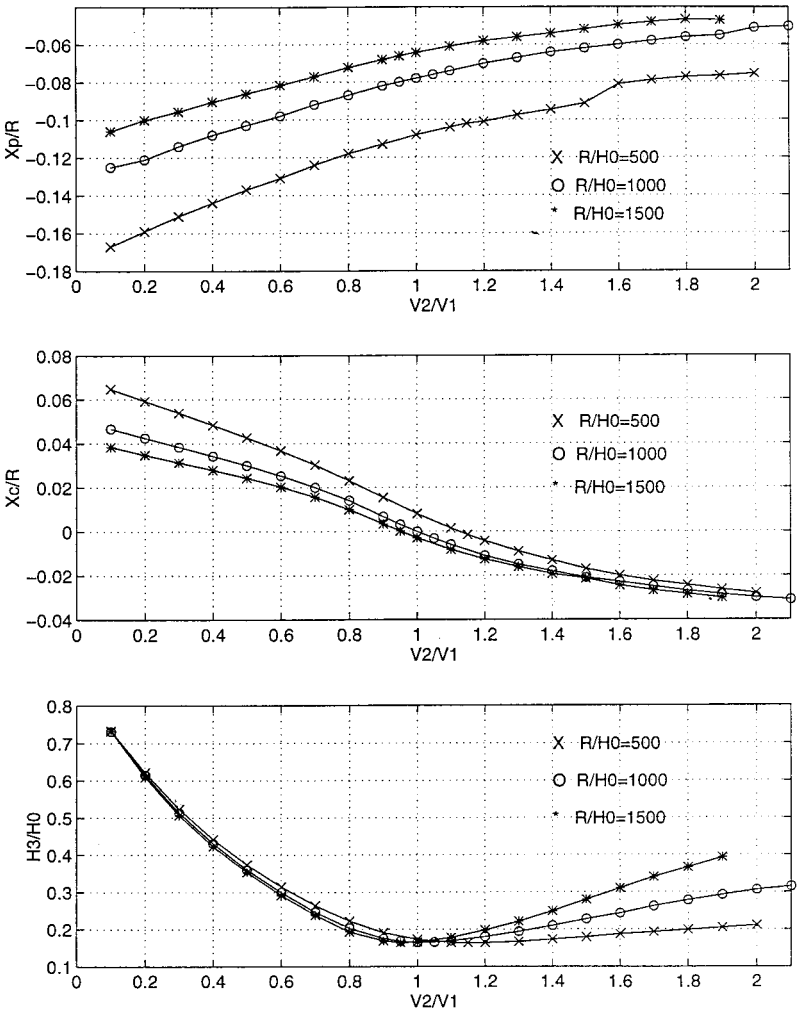

Figure 9. Effects of principal roll radius R/H_0 on reverse roll coating ($Re = 25$, $Ca = 0.1$, $H_1/H_0 = 1.25$, $R_2/R_1 = 1$ and $St = 0$).

In the past, no attempt was made to describe the role that the roll's radii play in either forward or reverse roll coating processes. In Figure 9 it is illustrated that the critical speed ratio tends to become slightly lower for smaller principal radii. Exceeding the critical speed ratio leads to an increase in film thickness that is more pronounced for larger principal radii. Thus, for a given speed ratio higher than the critical value, a thinner metered film can be achieved by means of decreasing the principal radius.

In practice, the two rolls are often of unequal radius. However, Figure 10 shows that roll radius ratio has no significant effect on reverse roll coating. Similarly, gravity effects can also be ignored.

As mentioned earlier in Section 3, the slip length and the apparent contact angle are empirical inputs. The former has little effect (Figure 11) while the latter has an important effect (Figure 12) on the reverse roll coating processes. Therefore, the predictions for reverse roll

coating processes are quantitatively accurate provided that the contact angle is available. Nevertheless, it is believed that the predicted general features and trends of reverse roll coating are not affected by varying input values of slip length and contact angle, as seen in Figures 11 and 12. For example, a minimum metered film thickness exists and is always achieved when the contact line passes through the gap centre, regardless of the chosen slip length and the apparent contact angle. It is also found that metered film thickness sensitivity to the apparent contact angle becomes significant only at high speed ratios.

In addition, the current calculations indicate that in the creeping flow regime ($Re = 0$) or at high capillary number ($Ca > 1$), increasing the speed ratio beyond the critical value makes it difficult to remove oscillations of $\Delta\alpha$ in a region close to the upstream side free surface. So far, we do not know whether this observation arises from the computational method itself or is related to a real flow instability.

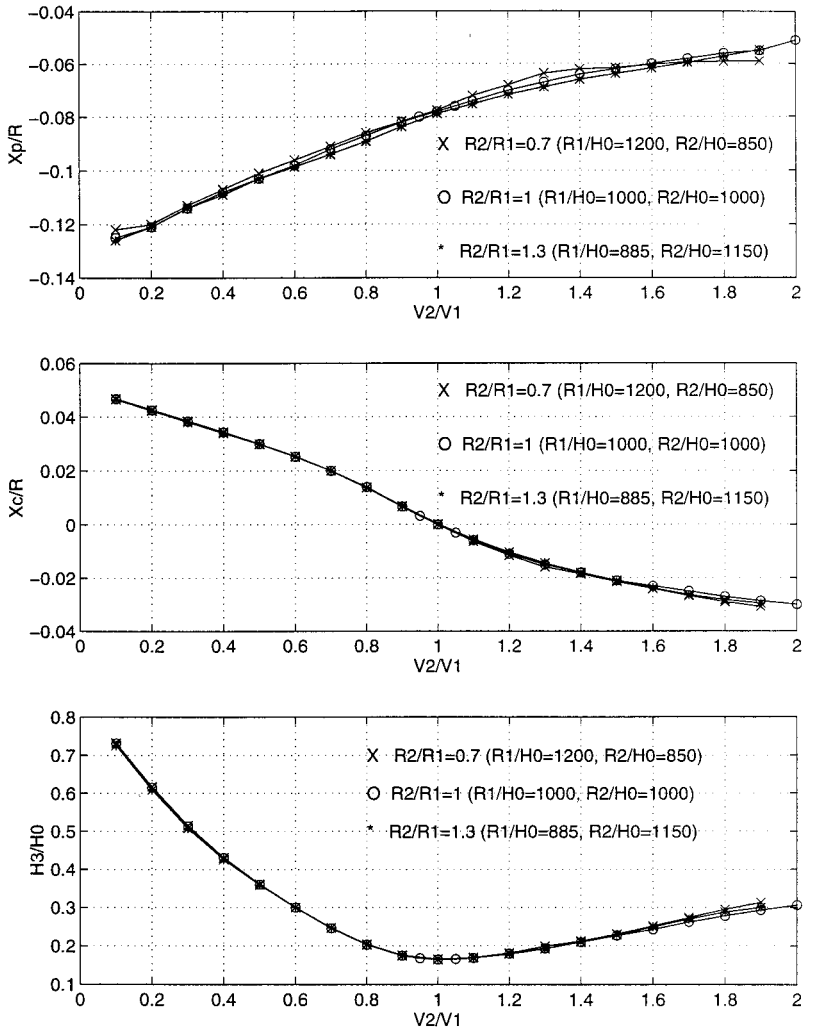

Figure 10. Predicted upstream side free surface position X_p/R, contact line position X_c/R and metered film thickness H_3/H_0 with variations of roll radius ratio R_2/R_1 ($Re = 25$, $Ca = 0.1$, $H_1/H_0 = 1.25$, $R/H_0 = 1000$ and $St = 0$).

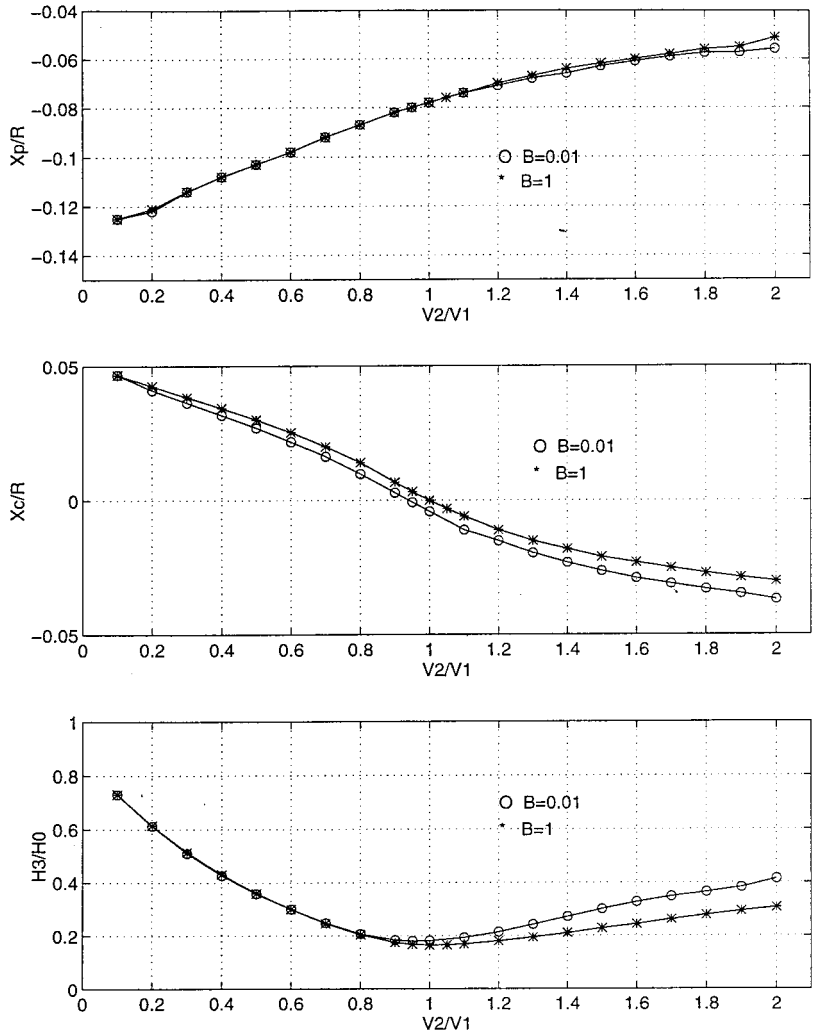

Figure 11. Effect of slip coefficient (slip length) B on finite element solutions ($Re = 25$, $Ca = 0.1$, $H_1/H_0 = 1.20$, $R/H_0 = 1000$, $R_2/R_1 = 1$ and $St = 0$).

Some of the above mentioned features, including the existence of a minimum metered film thickness at the critical speed ratio and effects of Reynolds and capillary number, are also in qualitative agreement with the experimental and computational results obtained by Coyle *et al.* [5]. Since the complete set of parameters used in their work is not provided, comparison of the current solutions with their results is not available at this time.

6. CONCLUDING REMARKS

A finite element solution of the Navier–Stokes equation for steady, two-dimensional, Newtonian free surface flows in reverse roll coating has been presented. It provides comprehensive predictions of the flow field for an apparent contact angle of 110°.

It reveals the general features of reverse roll coating. Namely, as the speed ratio increases, the dynamic contact line is drawn into the gap while the upstream side free surface shrinks further towards the gap and becomes highly curved. When the dynamic contact line passes through the gap, metered film thickness goes through a minimum and begins to increase continuously. The minimum of the metered film thickness occurs at certain roll speed ratio, defined as the critical speed ratio, which accounts for the transition value from lower to higher speed ratio range. The contact line exactly lies in the gap centre between two coating rolls when the critical speed ratio is reached. These phenomena are independent of any other parameters, including slip coefficient (slip length) and apparent contact angle.

Variations of other parameters, such as the Reynolds number, the capillary number, the arriving film thickness, the principal roll radius and so on, have lead to the following conclusions:

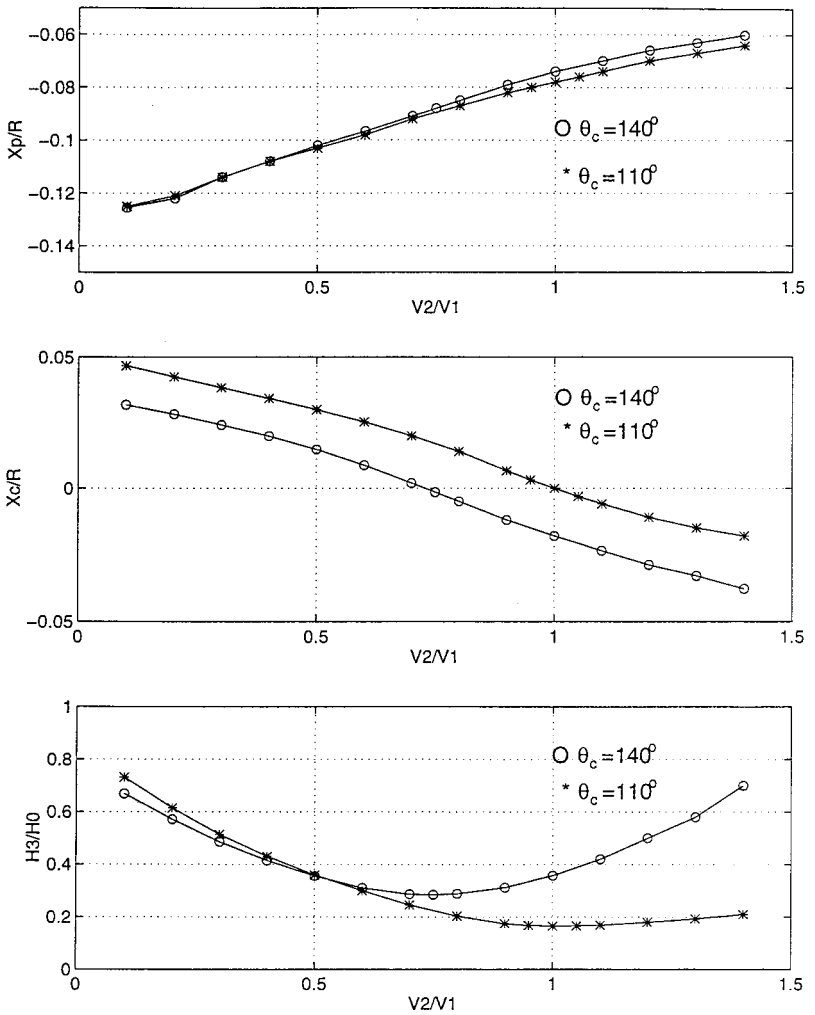

Figure 12. Effects of the contact angle θ_c on the finite element solutions ($Re = 25$, $Ca = 0.1$, $H_1/H_0 = 1.25$, $R/H_0 = 1000$, $R_2/R_1 = 1$ and $St = 0$).

- Decreasing the Reynolds number causes the critical speed ratio to have a lower value and the contact line to locate further towards the upstream side free surface. Slight effects of the Reynolds number are detected at lower speed ratios and stronger deviations ensue when upturn of metered film thickness occurs. The smaller the Reynolds number is, the steeper the film thickness upturn becomes and the more difficult it is to maintain a stable solution for the coating process at speed ratios beyond the critical value.
- The capillary number is an important factor, greatly influencing the flow field of reverse roll coating. At lower speed ratios, smaller capillary numbers result in thicker metered film while the opposite is true at higher speed ratios.
- The arriving film thickness strongly affects the metered film thickness and the dynamic contact line position if the speed ratio is beyond the critical value. This is particularly true for the case of arriving film thickness ratios smaller than unity. Thinner arriving films always cause the upstream side free surface to be drawn to the minimum gap and the metered film to become thicker.
- The principal roll radius plays a comparatively important role in reverse roll coating at high speed ratios. For high speed ratios, the contact line location is not altered greatly. For speed ratios beyond the critical point, a much thinner metered film can be obtained by using coaters with smaller principal roll radius.
- Within practical parameter value range, both the roll radius ratio and gravity (in terms of Stokes number) have no significant effects on reverse roll coating.

The foregoing results may also provide valuable information and a knowledge base for further study on flow instabilities in reverse roll coating or other challenging topics, such as the electrophoretic motion of charged particles in the flow field generated by two reversely rotating rolls.

ACKNOWLEDGMENTS

This work is part of Y. Hao M.Sc. Thesis submitted to the Senate of the Technion.

APPENDIX A. NOMENCLATURE

B	dimensionless slip coefficient ($\beta\mu/H_0$)
Ca	capillary number $\mu V_1/\sigma$
$\mathbf{f}$	unit vector in the direction of the gravity
F	total number of free surface nodes
g	gravity acceleration
h	scalar element of $\mathbf{h}$
$\mathbf{h}$	vector of free surface parameters
H_0	minimum gap between two rolls
H_1	thickness of arriving film
H_2	thickness of transferred film
H_3	thickness of metered film
$\mathbf{I}$	unit dyadic
$\mathbf{J}$	Jacobian matrix
J_0	Jacobian of isoparametric transformation
K	total number of velocity nodes
L	total number of pressure nodes

$\mathbf{n}$	unit vector normal to the surface
p	dimensionless pressure
P	pressure
P_a	ambient pressure
$\mathbf{R}$	vector of Galerkin weighted residuals
R	principal roll radius $[2/(1/R_1+1/R_2)]$
R_1	radius of roll 1
R_2	radius of roll 2
Re	Reynolds number $(\rho V_1 H_0/\mu)$
s	arc length along the boundary surface
St	Stokes number $(\rho g H_0^2/\mu V_1)$
$\mathbf{t}$	unit vector tangential to the surface
$\mathbf{T}$	total stress
$\mathbf{u}$	dimensionless velocity
u	x component of dimensionless velocity
$\mathbf{U}$	velocity field
v	y component of dimensionless velocity
V_1	peripheral velocity of roll 1 (applicator roll)
V_2	peripheral velocity of roll 2 (metering roll)
x, y	dimensionless Cartesian co-ordinates in physical domain
X, Y	Cartesian co-ordinates in physical domain
X_c	dynamic contact line position
X_p	relative position of the upstream side free surface defined by the distance between the free surface and the gap centre between the two rolls

Greek letters

α	vector of finite element coefficients
β	local slip coefficient
ϵ	convergence constant
θ_c	apparent contact angle
μ	fluid viscosity
ξ, η	Cartesian co-ordinates in computational domain
ρ	fluid density
σ	surface tension
$\boldsymbol{\tau}$	dimensionless stress
Φ^k	biquadratic basis function
Ψ^l	bilinear basis function

Superscripts

f	free surface node
k	velocity nodes
l	pressure nodes

Subscripts

C	continuity weighted residual
f	free surface
in	inlet boundary

K	kinematic weighted residual
M	momentum weighted residual
n	iteration times
s	solid surface
x	x component
y	y component

REFERENCES

1. H. Benkreira, M.F. Edwards and W.L. Wilkinson, 'A semi-empirical model of the forward roll coating of Newtonian fluids', *Chem. Eng. Sci.*, **36**, 423 (1981).
2. H. Benkreira, M.F. Edwards and W.L. Wilkinson, 'Roll coating of purely viscous liquids', *Chem. Engng. Sci.*, **36**, 429 (1981).
3. D.G. Higgins, 'Coating methods—survey', *Encyclo. Polym. Sci. Technol.*, **3**, 765 (1965).
4. G.L. Booth, *Coating Equipments and Processes*, Lockwood Publishing, New York, 1970.
5. D.J. Coyle, C.W. Macosko and L.E. Scriven, 'The fluid dynamics of reverse roll coating', *AIChE J.*, **36**, 161 (1990).
6. D.J. Coyle, C.W. Macosko and L.E. Scriven, 'A simple model of reverse roll coating', *Ind. Eng. Chem. Res.*, **29**, 1416 (1990).
7. J. Greener and S. Middleman, 'Theoretical and experimental studies of the fluid dynamics of a two-roll coater', *I&EC Fund.*, **18**, 35 (1979).
8. M. Decré, E. Gailly and J.M. Buchlin, 'Meniscus shape experiments in forward roll coating', *Phys. Fluids*, **7**, 458 (1995).
9. E. Pitts and J. Greiller, 'The flow of thin liquid films between rollers', *J. Fluid Mech.*, **11**, 33 (1961).
10. J.C. Hintermaier and R.E. White, 'The splitting of water film between rotating rolls', *TAPPI*, **48**, 617 (1965).
11. H. Benkreira, M.F. Edwards and W.L. Wilkinson, 'Flux distribution in forward roll coating: a simple analysis', *Chem. Eng. J.*, **25**, 211 (1982).
12. D.J. Coyle, C.W. Macosko and L.E. Scriven, 'Film-splitting flows in forward roll coating', *J. Fluid Mech.*, **171**, 183 (1986).
13. D.J. Coyle, C.W. Macosko and L.E. Scriven, 'Film-splitting flows of shear thinning liquids in forward roll coating', *AIChE J.*, **33**, 741 (1987).
14. P.H. Gaskell, M.D. Savage, J.L. Summers and H.M. Thompson, 'Modelling and analysis of meniscus roll coating', *J. Fluid Mech.*, **298**, 113 (1995).
15. M.S. Carvalho and L.E. Scriven, 'Multiple states of a viscous fill surface flow: transition from pre-metered to a metering inflow', *Int. J. Numer. Methods Fluids*, **24**, 813 (1997).
16. W.S. Ho and F.M. Holland, 'Between roll metering coating technique, a theoretical and experiment study', *TAPPI*, **61**, 53 (1978).
17. J. Greener and S. Middleman, 'Reverse roll coating of viscous and viscoelastic liquids', *I&EC Fund.*, **20**, 63 (1981).
18. E.B. Dussan, 'The moving contact line: the slip boundary condition', *J. Fluid Mech.*, **77**, 665 (1976).
19. E.B. Dussan and S.H. Davis, 'On the motion of a fluid–fluid interface along a solid surface', *J. Fluid Mech.*, **65**, 71 (1974).
20. L.M. Hocking, 'A moving flow interface on a rough surface', *J. Fluid Mech.*, **76**, 801 (1976).
21. L.M. Hocking, 'A moving fluid interface. Part 2. The removal of the force singularity by a slip flow', *J. Fluid Mech.*, **79**, 209 (1977).
22. C. Huh and L.E. Scriven, 'Hydrodynamic model of steady movement of a solid/liquid/fluid contact line', *J. Coll. Interface Sci.*, **35**, 85 (1971).
23. S.F. Kistler and L.E. Scriven, 'Coating flows', in J.R. Pearson and S.M. Richardson (eds.), *Computational Analysis of Polymer Processing*, Applied Science Publishers, London, 1983.
24. S.F. Kistler and L.E. Scriven, 'Coating flow theory by finite element and asymptotic analysis of the Navier–Stokes system', *Int. J. Numer. Methods Fluids*, **4**, 207 (1984).
25. K.J. Ruschak, 'A method for incorporating free boundaries with surface tension in finite element fluid flow simulators', *Int. J. Numer. Methods Eng.*, **15**, 639 (1980).
26. O.C. Zienkiewicz, *The Finite Element Method*, 3rd edn., McGraw-Hill Book Company, New York, 1977.
27. IMSL MATH/LIBRARY: FORTRAN subroutines for mathematical applications, IMSL, Houston, 1989.

